Journal of Biomechanics 45 (2012) 842–849

Contents lists available at SciVerse ScienceDirect

Journal of Biomechanics

journal homepage: www.elsevier.com/locate/jbiomech
www.JBiomech.com

Mechanical changes in the rat right ventricle with decellularization

Colleen Witzenburg [a], Ramesh Raghupathy [a], Stefan M. Kren [b], Doris A. Taylor [b], Victor H. Barocas [c,*]

[a] Department of Mechanical Engineering, University of Minnesota, Minneapolis, MN 55455, USA
[b] Center for Cardiovascular Repair, Department of Integrative Biology and Physiology, University of Minnesota, Minneapolis, MN 55455, USA
[c] Department of Biomedical Engineering, University of Minnesota, 7-105 Nils Hasselmo Hall, 312 Church St SE, Minneapolis, MN 55455, USA

ARTICLE INFO

Article history:
Accepted 30 September 2011

Keywords:
Perfusion-decellularization
Heart ventricle
Heterogeneous
Biaxial testing

ABSTRACT

The stiffness, anisotropy, and heterogeneity of freshly dissected (control) and perfusion-decellularized rat right ventricles were compared using an anisotropic inverse mechanics method. Cruciform tissue samples were speckled and then tested under a series of different biaxial loading configurations with simultaneous force measurement on all four arms and displacement mapping via image correlation. Based on the displacement and force data, the sample was segmented into piecewise homogeneous partitions. Tissue stiffness and anisotropy were characterized for each partition using a large-deformation extension of the general linear elastic model. The perfusion-decellularized tissue had significantly higher stiffness than the control, suggesting that the cellular contribution to stiffness, at least under the conditions used, was relatively small. Neither anisotropy nor heterogeneity (measured by the partition standard deviation of the modulus and anisotropy) varied significantly between control and decellularized samples. We thus conclude that although decellularization produces quantitative differences in modulus, decellularized tissue can provide a useful model of the native tissue extracellular matrix. Further, the large-deformation inverse method presented herein can be used to characterize complex soft tissue behaviors.

1. Introduction

A bioartificial heart is a possible alternative to transplantation or a mechanical left ventricular assist device. Whole-organ perfusion-decellularization has been established as a potential tool to produce an intact three-dimensional scaffold for bioartificial hearts (Ott et al., 2008; Wainwright et al., 2010; Weymann et al., 2011). Separating the cells from the extracellular matrix also provides the opportunity to study cardiac wall mechanics in a simplified system, and attribute myocardial tissue properties to the respective cellular/extracellular constituents. For instance, localized matrix injury or scarring that occurs in myocardial infarction (Fomovsky and Holmes, 2010; Chen et al., 2003) could be studied on the extracellular matrix with decellularized tissue.

Previous studies of healthy and/or infarcted myocardium have focused on constitutive modeling of small samples cut from different locations to assess heterogeneity while assuming homogeneity in each sample (e.g. Sacks and Chuong, 1993; Emery et al., 1997). Assessing heterogeneity by means of multiple samples is impossible, however, if the entire tissue is too small. For example, the ventricle of the Sprague-Dawley (SD) rat, a popular choice for myocardial decellularization experiments (Ott et al., 2008), is only about 10 mm across and not amenable to assessment of heterogeneity with samples cut from different locations. Although indentation (e.g. Cox et al., 2010) could be applied regionally, it is less relevant to in vivo function. An experiment in which heterogeneous properties could be extracted from a single sample during biaxial loading would be far more valuable.

The generalized anisotropic inverse mechanics (GAIM) method (Raghupathy and Barocas, 2010; Raghupathy et al., 2011) enables study of heterogeneous, anisotropic tissues, like the ventricle, by dissecting small samples computationally rather than physically. GAIM directly solves the finite element representation of the stress balance in the tissue for the unknown components of the two-dimensional general linear elasticity tensor. Heterogeneity within the sample is managed by partitioning the sample into many subdomains, each assumed to have uniform properties. In this study, we utilized multiple biaxial tests and an extended version of GAIM to determine the mechanical properties of freshly dissected (control) and decellularized right ventricles from SD rats. We focused on the right ventricle due to the prohibitively large thicknesses of control left ventricle samples.

Two hypotheses were tested. First, since the extracellular matrix, particularly collagen, plays a large role in tissue mechanical behavior (Fomovsky et al., 2010), and since decellularization reduces tissue volume considerably with negligible collagen loss (Ott et al., 2008), we hypothesized that *decellularized samples would have larger stiffness values for the right ventricle as measured by our methods.* We expected this increase in stiffness to be proportional to the thickness reduction, as observed previously

* Corresponding author. Tel.: +1 612 626 5572; fax: +1 612 626 6583.
E-mail address: baroc001@umn.edu (V.H. Barocas).

0021-9290/$ - see front matter © 2011 Elsevier Ltd. All rights reserved.
doi:10.1016/j.jbiomech.2011.11.025

(Ott et al., 2008). Second, based on minimal changes in the collagen structure following decellularization, we hypothesized that *decellularized samples would not exhibit a change in degree of mechanical anisotropy or heterogeneity.*

2. Methods

2.1. Sample Preparation

Whole cadaveric rat hearts were removed from ten adult female SD rats (9–13 weeks) for testing. All experiments were performed in accordance with US Animal Welfare Act and were approved by the Institutional Animal Care and Use Committee at the University of Minnesota. Five hearts underwent decellularization prior to ventricle dissection and five immediately underwent ventricle dissection (control). One sample from each group was discarded due to damage during experimentation; therefore, four samples from each group were analyzed. Measurements of live rat body weight prior to dissection showed no significant difference ($p=0.28$) between groups. Unless otherwise stated, all p-values reported refer to unpaired two-tailed t-tests.

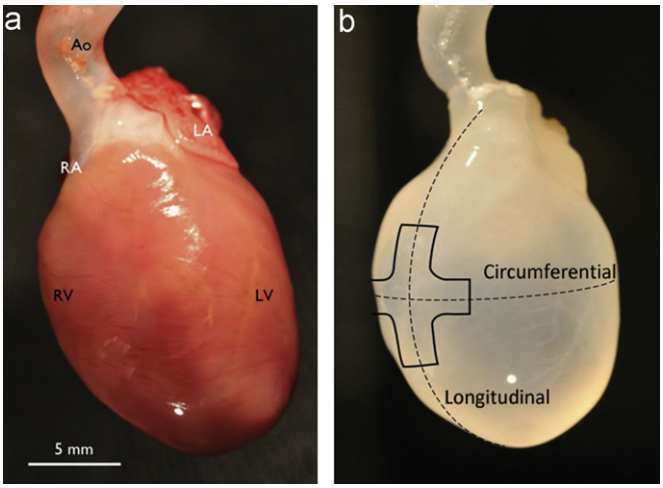

Fig. 1. Sample geometry. (a) Rat heart during decellularization. Labels indicate aorta (Ao), right atrium (RA), left atrium (LA), right ventricle (RV), and left ventricle (LV). (b) Sketch of sample geometry overlaid on fully decellularized rat heart, showing the circumferential and longitudinal directions.

For decellularization, hearts were placed in a modified Langendorff apparatus and perfused through the coronary arteries with 1% sodium dodecyl sulfate (SDS) in water for 20 h, as described previously (Ott et al., 2008). Each heart was then perfused with 60 ml deionized water, 60 ml 1% Triton-X100 in water, and 60 ml additional deionized water to flush the detergent. The hearts were then perfused with 500 ml phosphate buffered saline (PBS) in 5 aliquots, leaving only decellularized matrix behind. Fig. 1 shows a rat heart during decellularization and depicts where samples were cut from the right ventricle. Sample geometry is shown in Fig. 1b.

The right ventricle was dissected from each heart and laid flat. A punch was used to cut each sample into a cruciform shape for biaxial testing. Anatomical orientation was marked on the endocardial surface as shown in Fig. 2a. Samples were stored in 1% PBS at 4 °C when not undergoing biaxial testing or thickness measurement. Sample thickness was measured by laser micrometer 5 min after removal from PBS.

2.2. Biaxial testing

Samples were tested within 48 h of dissection. Verhoeff's stain was used to texture the epicardial surface for optical strain tracking (Fig. 2b). The textured sample was attached to an Instron biaxial tester with four 5 N load cells via a custom rig that allowed easy sample mounting and immersion in 1% PBS at room temperature for the duration of testing (Fig. 2c).

A series of biaxial protocols was applied to each sample. First, a slight preload, ~0.01 N, was applied to each cruciform arm. The grip forces were zeroed with respect to the preload. The sample was preconditioned with nine equibiaxial extensions; each of the four arms was extended 0.75 mm. Each loading and unloading cycle lasted 10 s. After preconditioning, fifteen separate displacement-controlled biaxial experimental extensions were performed (Fig. 3). Unlike traditional mechanical tests, which are designed to maximize homogeneity of the strain field, our protocol was designed to produce many heterogeneous strain fields and to vary that heterogeneity over different tests. Heterogeneous, variable strain fields are necessary to provide detailed deformation data for GAIM, and using numerous fields improves the accuracy of parameters. An additional

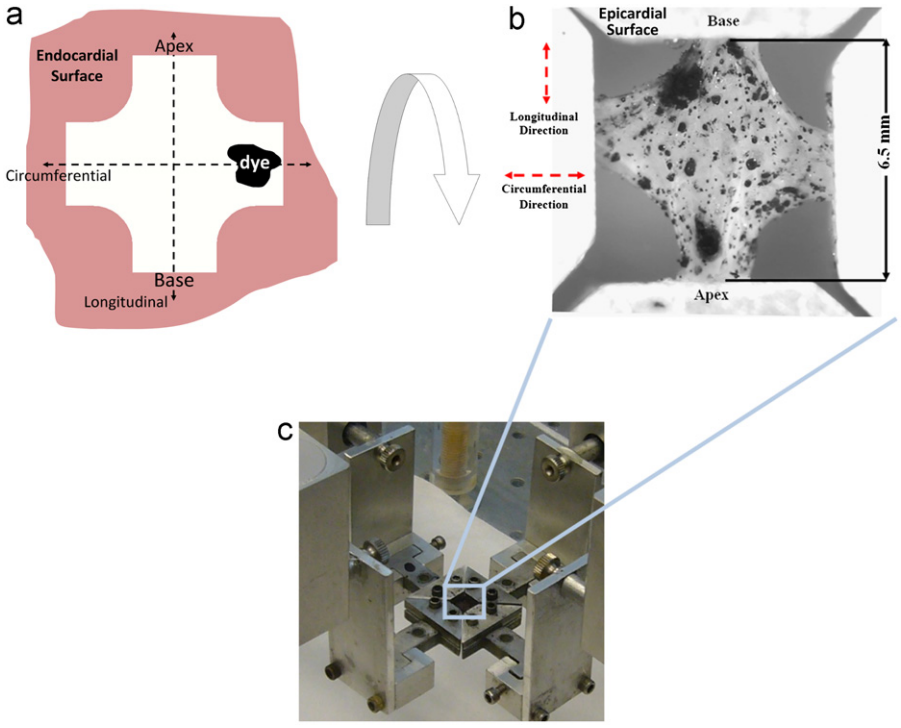

Fig. 2. Sample dissection and clamping. (a) Schematic showing the anatomical position of the tissue during punching. (b) Epicardial surface of a representative decellularized right rat ventricle after clamping and speckling. (c) Clamping configuration during biaxial testing. The sample is submerged in 1% phosphate buffered saline at room temperature.

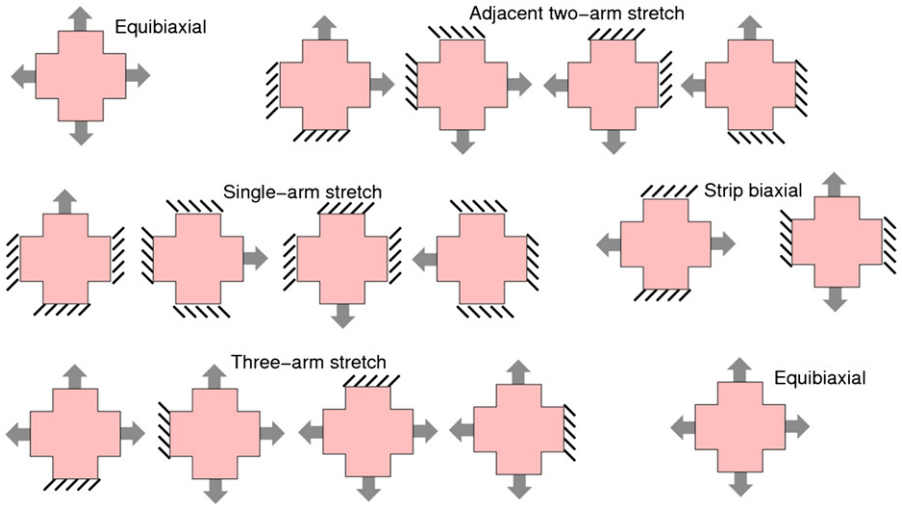

Fig. 3. Protocol used for the biaxial testing of each sample. Dashed lines indicate fixed arms. Equibiaxial: each arm moved 0.75 mm. Adjacent two-arm stretch: extended arms moved 1.0 mm. Single–arm stretch: extended arm moved 1.0 mm. Strip biaxial: extended arms moved 0.75 mm. Three-arm stretch: middle extended arm moved 1.0 mm, other extended arms moved 0.75 mm.

equibiaxial extension was performed at the end of testing to confirm that minimal damage had occurred during the experiment. During testing, images of the epicardial surface of the tissue and the forces at each grip were recorded.

2.3. Image analysis and strain tracking

Digital video of ventricle deformation was obtained at 24 fps, 1080p HD resolution, and spatial resolution of ~96 pixels/mm. The video was synchronized and downsampled to construct grayscale image sequences corresponding to the loading curves of each test. The image at the end of preconditioning was used as the reference configuration. The tissue boundary was sketched on top of the reference image in Abaqus™, and meshed with quadrilateral elements. Successive pairs of images were correlated to track the movement of the mesh nodes throughout the loading sequence. This image correlation method was used successfully in Raghupathy et al. (2011). Displacement fields were constructed from movement of locations corresponding to the mesh nodes and smoothed to reduce noise. Green strains were computed from cumulative displacement fields by standard finite element theory for bilinear quadrilateral elements. We estimated the accuracy of our displacement calculations by digitally deforming the image of Fig. 2b and comparing the displacements obtained from image correlation with analytical values. Displacements were accurate to ± 0.06 pixels and the strains to ± 0.0026 (95% CI).

2.4. Generalized anisotropic inverse mechanics (GAIM)

Regional mechanical properties were determined by an extension of our GAIM method (Raghupathy and Barocas, 2010; Raghupathy et al., 2011). The method, presented in more detail in our previous work, involves solving the direct inverse problem for a general linear elastic solid. That is, given the displacement data and forces on the sample grips, the method uses finite elements to solve the linear elastic stress balance $(C_{ijkl}\varepsilon_{kl})_{,j}=0$ for the components of C. The domain is partitioned into regions, over each of which C is taken to be a constant. The partitions are optimized so as to minimize error in the force balance while maintaining tight confidence intervals on the components of C (Raghupathy and Barocas, 2010). All experiments within the protocol are evaluated concurrently to produce a large, overdetermined system of linear equations for C.

For highly deformable tissues such as myocardium, a formulation that accounted for large-deformation kinematics but maintained the generality, anisotropy, and linearity of the regression problem from our previous work was desired. We modified our original form to

$$S_{ij} = K_{ijkl}E_{kl} \tag{1}$$

where S is the 2nd Piola–Kirchhoff stress, E the Green strain, and K an elasticity tensor analogous to C in linear elasticity and has the same major and minor symmetries. The stress balance is

$$(F_{mi}S_{ij})_{,j} = (F_{mi}K_{ijkl}E_{kl})_{,j} = 0 \tag{2}$$

where F is the deformation tensor, and differentiation is with respect to the undeformed coordinates. Eq. (2), although nonlinear in the displacements, is linear with respect to the components of K, so the problem can be treated with linear regression theory (Raghupathy and Barocas, 2010). Thus, the nonlinear kinematics are incorporated into the analysis, but the fitting problem remains linear.

In our earlier work, the tensor C was used to identify the major features of the tissue. Specifically, the eigentensors of C represent principal states of stress and strain (Cowin and Mehrabadi, 1995; Thomson, 1856), and the corresponding eigenvalues (Kelvin moduli) provide measures of material stiffness. We have found (Raghupathy et al., 2011) that the largest Kelvin modulus is a useful measure and was comparable to Young's modulus for polydimethylsiloxane. A second important measure comes from the eigenvectors of the eigentensor corresponding to the largest Kelvin modulus. These eigenvectors describe the anisotropy of the material, with the direction corresponding to the larger eigenvalue aligning with the tissue fiber direction in theoretical studies (Raghupathy and Barocas, 2010), on a simple fiber model (Raghupathy and Barocas, 2009), and in experiments on cell-compacted collagen gels (Raghupathy et al., 2011).

In the current work, we computed large-deformation analogs of the Kelvin moduli (henceforth simply "Kelvin moduli" for brevity) and corresponding principal directions which give the preferred stiffness direction (θ). In addition, the eigenvalues of the principal eigentensor of K, λ_1, and λ_2 were converted into an anisotropy index (r), indicating strength of the alignment. It varies from 0 for an isotropic sample to 1 for a perfectly aligned sample:

$$r = \frac{|\lambda_1| - |\lambda_2|}{|\lambda_1| + |\lambda_2|} \tag{3}$$

In addition to stiffness and alignment, we quantified tissue heterogeneity by calculating the standard deviation of each variable over all partitions within the center of the sample. That is, each partition was treated as an independent measurement, and the standard deviation was calculated. We refer to this value as the "partition standard deviation" to avoid confusion with measures of sample-to-sample variability.

3. Results

Right ventricle wall thickness was 2138 ± 527 μm (mean $\pm$ 95% CI) for controls and 381 ± 157 μm for the decellularization group ($p < 10^{-4}$). This was expected since cellular material comprises much of the tissue volume. When the first and final equibiaxial protocol strain maps were compared they showed extremely similar patterns and values. There was no significant difference between the protocols in peak force for any arm of any sample ($p > 0.1$ for all samples, paired two-tailed t-test).

Loading behavior for a representative sample of decellularized tissue (Fig. 2b) is shown in Fig. 4. Fig. 4b and c highlight a displacement-controlled equibiaxial test and single-arm extension test. For equibiaxial loading, the circumferential arms, right and left, had higher loads than the longitudinal arms, top and bottom. Shear forces were responsible for the discrepancy in force between

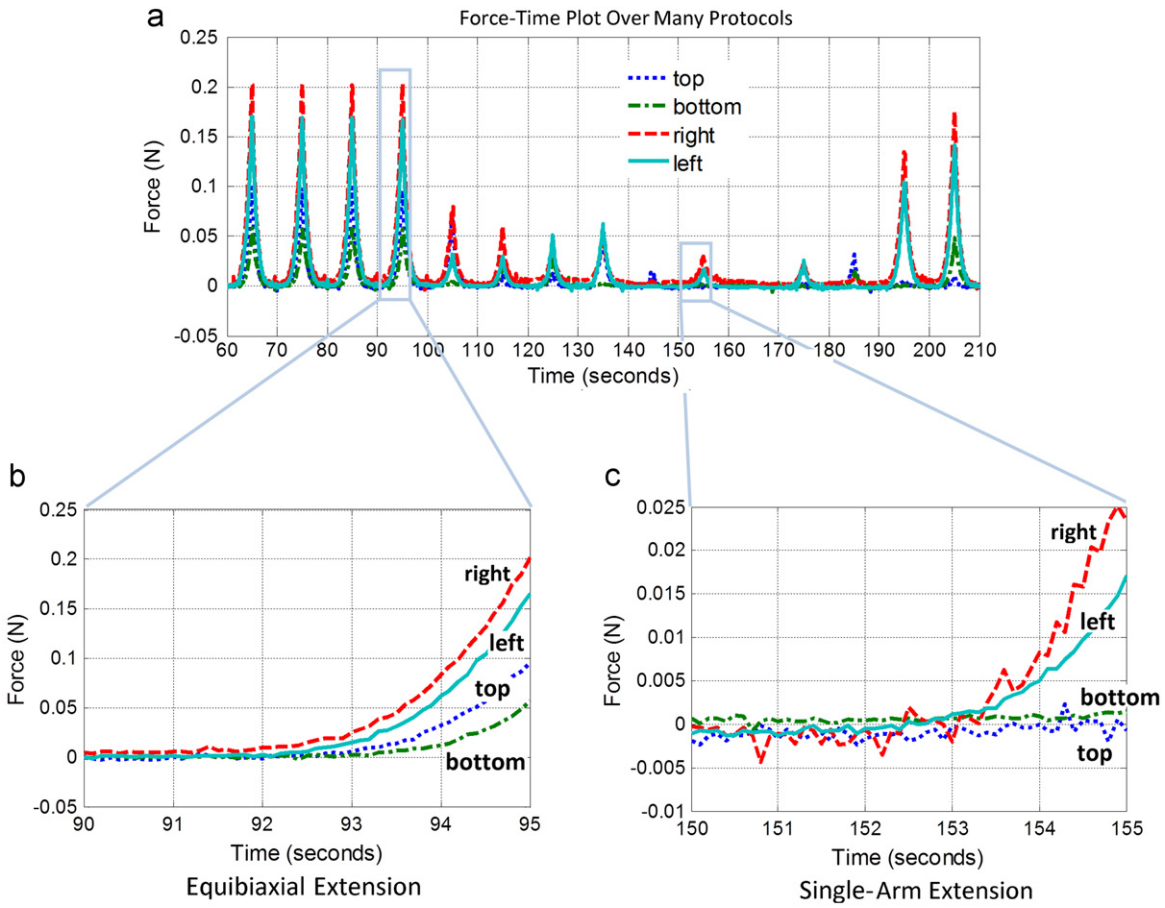

Fig. 4. Representative load data for the decellularized sample shown in Fig. 2b. (a) Three of nine preconditioning cycles are shown followed by the equibiaxial protocol, four adjacent two-arm extension protocols, four single-arm extension protocols, two strip biaxial protocols and one three-arm extension protocol. Other protocols not shown. (b) During equibiaxial loading, significant forces were generated in all four arms, with higher forces in the circumferential (left–right) direction because of tissue anisotropy. (c) When only the right arm was displaced, all forces were much smaller, and circumferential forces were much larger than longitudinal forces.

opposite arms. The single-arm extension involved displacement of the right arm, as indicated by large forces on that arm and the reduced response of the left arm. Forces on the top and bottom arms were small in comparison.

For the same sample, the Green strains – E_{xx}, E_{yy} and E_{xy} – at peak displacement for both equibiaxial and single-arm extension tests are shown in Fig. 5. For the equibiaxial test, strain was larger in the vertical direction than in the horizontal direction in the central region of the sample. This effect was reversed for the single-arm extension test. Also, E_{yy} showed a strong horizontal gradient across the central region of the sample for the single-arm extension (Fig. 5e). Thus, as desired, strain fields were heterogeneous and the strain differed within the same region of the sample from one protocol to another. For both tests, however, there was relatively little shear strain.

Alignment and stiffness maps were calculated for each sample using the extended GAIM method. Fig. 6 shows maps for the sample pictured in Fig. 2b. The arms of the sample present as artificially aligned in the pull direction as a result of our inability to measure transverse forces on the grips and minimal transverse displacement in the arms. However, the central region of the sample is well-specified, so our analysis focuses only on the central region (Fig. 6b, d).

Fig. 6a shows strong circumferential (i.e., left–right) alignment in the central region. The average value of the anisotropy index within the central region (Fig. 6b) was 0.71, indicating strong anisotropy (roughly five times stiffer in the preferred, i.e. circumferential, direction). The partition standard deviation for the anisotropy index was low, 0.084. The average value for the preferred stiffness direction within the central region was 7.66° from the horizontal, and its partition standard deviation was 7.55°. Fig. 6c shows the maximum Kelvin modulus within each region. The average value of the maximum Kelvin modulus within the central region (Fig. 6d) was 400 kPa, and its partition standard deviation was 107 kPa.

Fig. 7 summarizes the GAIM results for this study. Fig. 7a–c show the average values of maximum Kelvin modulus, $\langle E_k \rangle$, anisotropy index, $\langle r \rangle$, and preferred stiffness direction, $\langle \theta \rangle$, over the central region. There was significant difference between $\langle E_k \rangle$ for the control and decellularized groups ($p=0.0003$), indicating that the central region of the decellularized tissue was stiffer than that of the control. However, there was no significant difference between $\langle r \rangle$ or $\langle \theta \rangle$ for the control and decellularized groups ($p=0.06$, 0.31), indicating no change in strength or direction of anisotropy. All samples were stiffer in the circumferential than the longitudinal direction.

Fig. 7d–f show the normalized partition standard deviations of the maximum Kelvin modulus, $\sigma_{Ek}/\langle E_K \rangle$, anisotropy index, $\sigma_r/\langle r \rangle$, and preferred stiffness direction, $\sigma_\theta/\langle \theta \rangle$, over the central region. These values were used to quantify the degree of

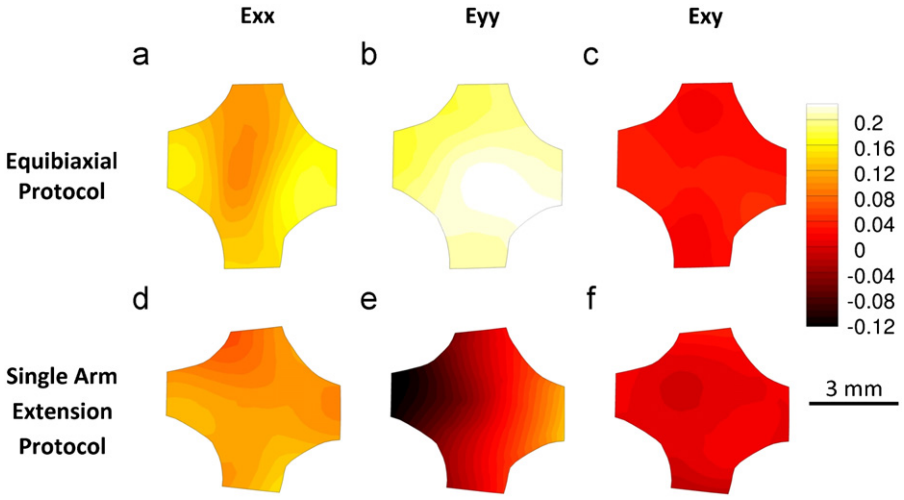

Fig. 5. Representative strain results for the decellularized sample shown in Fig. 2b. Strains are overlaid on the deformed sample shape at maximum deformation. During equibiaxial loading (a, b), the vertical strain (E_{yy}) was larger than the horizontal strain (E_{xx}) in the central region of the sample. During single-arm loading (d, e), E_{xx} was larger in the central region of the sample. Also, there was a gradient in the central region of the sample in the map for E_{yy}. In both cases, there was relatively little shear strain (c, f).

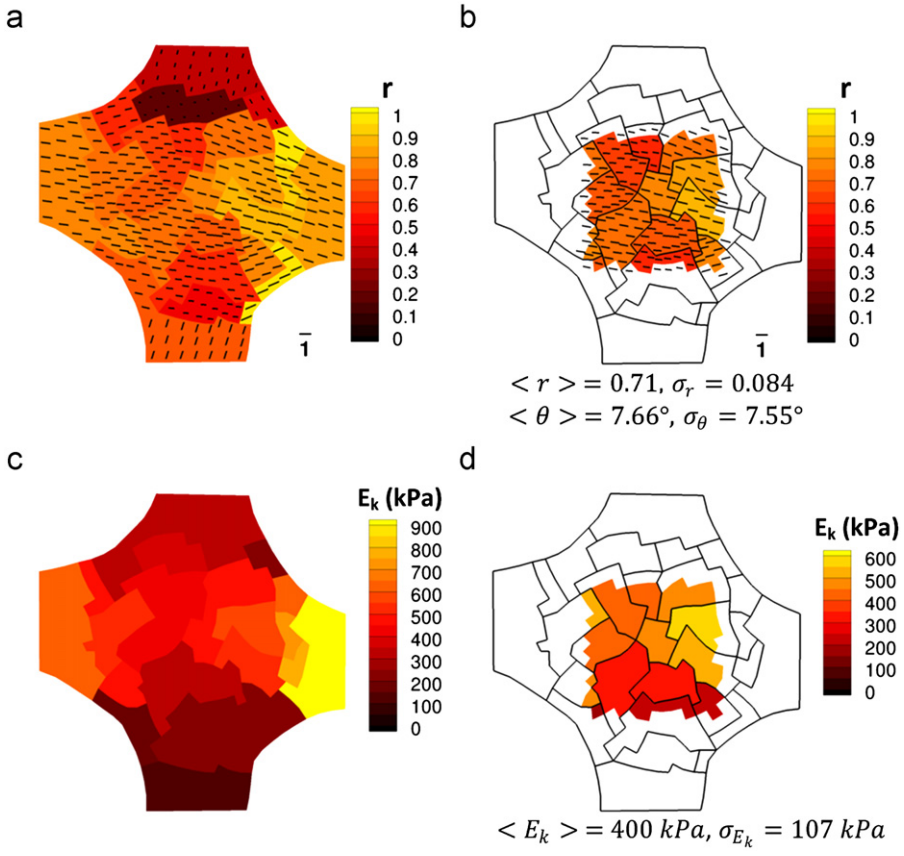

Fig. 6. Representative alignment and stiffness results from GAIM for the decellularized sample shown in Fig. 2b. Results are overlaid on the undeformed shape. For the alignment maps (a, b), the color shows the anisotropy index, and the vectors indicate the preferred stiffness direction, with vector lengths corresponding to the anisotropy index. For the stiffness maps (c, d) the contour shows the maximum Kelvin modulus. (a) Alignment map shows roughly uniform alignment in the center of the sample. (b) There was strong circumferential alignment in the central region of the tissue, $\langle r \rangle = 0.71$, with low partition standard deviation $\sigma_r = 0.084$, and $\langle \theta \rangle = 7.66°$, with a low partition standard deviation of $\sigma_\theta = 7.55°$. Black blocks indicate partition domain. (c) Stiffness map shows roughly uniform E_k in the center of the sample. (d) The average value of the maximum Kelvin modulus within the central region of the sample, $\langle E_k \rangle = 400$ kPa, and the partition standard deviation, $\sigma_{E_k} = 107$ kPa. Black blocks indicate partition domain.

heterogeneity of the parameters. For all three measures of heterogeneity (associated with stiffness, degree of anisotropy, and preferred direction) the control and decellularized samples gave statistically indistinguishable results ($p = 0.22, 0.76, 0.11$), indicating no significant change in heterogeneity between the decellularized and control groups.

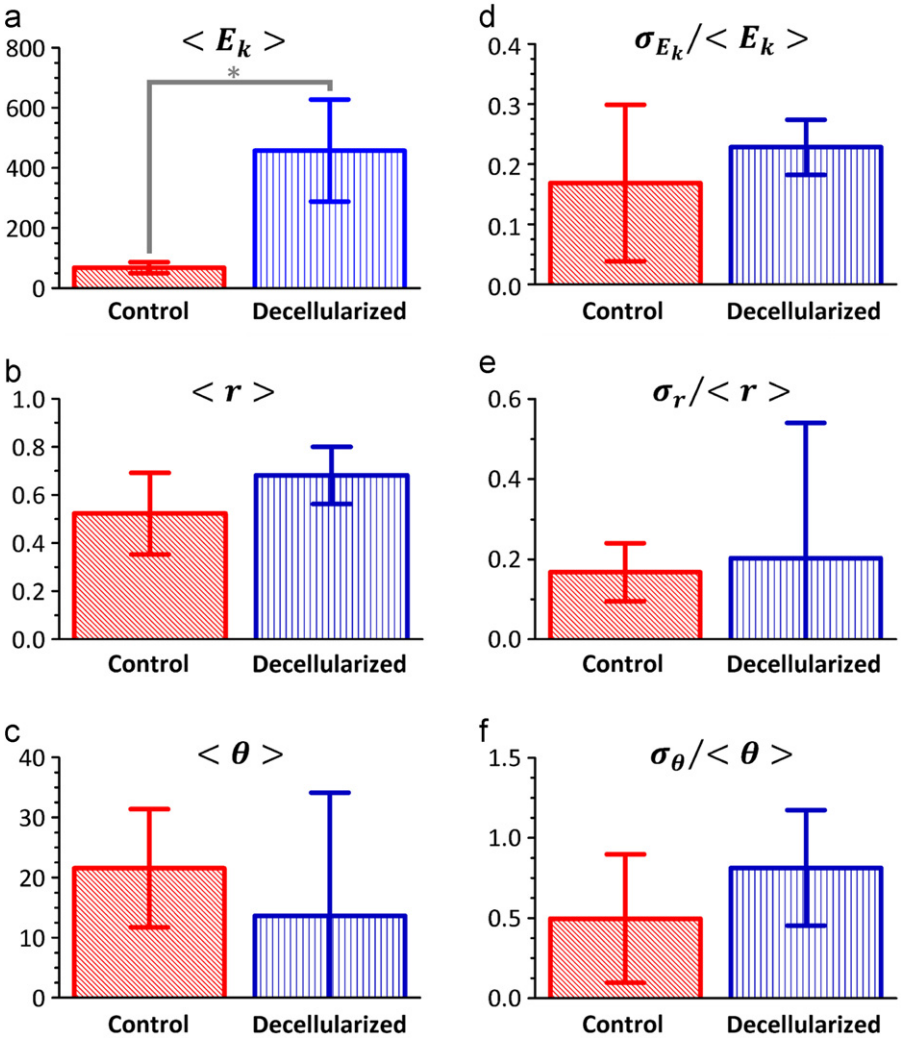

Fig. 7. Stiffness, alignment and direction results for full study. (a) There was a significant difference between the control and decellularized groups in $\langle E_k \rangle$, which indicates overall stiffening of the tissue with decellularization. Units of $\langle E_k \rangle$ are kPa. (b, c) No significant difference in $\langle r \rangle$ or $\langle \theta \rangle$ was found between the control and decellularized samples, indicating minimal change in anisotropy. Units of $\langle \theta \rangle$ are degrees and $\langle r \rangle$ is unitless. (d, e, f) No significant difference was found between the normalized partition standard deviation of the maximum Kelvin modulus, anisotropy index or preferred stiffness direction. This indicates that the effect of decellularization is roughly uniform. All plots show mean $\pm$ 95% CI, $n=4$.

4. Discussion

The major technical advance of this work was introduction of a nonlinear kinematic framework to the GAIM technique. The new formulation, which relates the second Piola–Kirchhoff stress to the Green strain linearly, maintains the efficiency of a linear regression model (i.e., the model is linear in the coefficients) but is suitable to large deformations often experienced by soft tissues. By doing so, we extended the potential applicability of the method to a wider range of soft-tissue applications. The generalized model is not sufficient to capture many soft-tissue behaviors, including the large toe region followed by a sharp rise in stiffness, but it provides a qualitative estimate of the material properties and, most importantly, an assessment of material anisotropy in different regions of an intact sample.

The major conclusions of this work as to the tissues tested were as follows: (1) The stiffness of right ventricular tissue, as measured by the average of the largest Kelvin modulus over the sample's center, increased by a factor of 6.7 with decellularization. This change was consistent with densification of the tissue (average 5.6-fold reduction in thickness) and was similar to that reported by others for decellularized cardiac tissue (Ott et al., 2008; Wang et al., 2010). Although other factors (e.g., chemical interactions between decellularizing agents and the extracellular matrix) could be important, we attribute the slightly larger increase in stiffness than decrease in thickness to structural changes, specifically rotation of collagen fibers into the plane of testing. (2) The mechanical anisotropy of the tissue, which we have shown previously (Raghupathy et al., 2011) to correlate to structural anisotropy, was largely unchanged by the decellularization process. (3) Finally, a key goal of this work was to assess tissue heterogeneity. We found that the spatial variation in tissue properties (stiffness, degree of anisotropy, and preferred stiffness direction) over the central region of the sample was largely unchanged by the decellularization process. Based on these three observations, we conclude that decellularized tissue can be used as a model for studying mechanical changes to the extracellular matrix in the heart. The decellularized model is particularly attractive for studies of rat left ventricle, which is sufficiently thick ($\sim$4 mm) relative to the other tissue dimensions ($\sim$10 mm) that planar biaxial tests would be of questionable validity. In the decellularized sample, the thickness is 5–10% of the in-plane dimensions, making the assumptions underlying planar biaxial tests much more acceptable. Of course, the decellularized model

does not allow for the study of the cells, but the combination of the decellularized system and GAIM analysis could allow assessment of mechanical consequences of ventricular remodeling (e.g., scar formation) without isolation of the remodeled tissue. Another potential advantage of the decellularized model is that, by virtue of being thinner, it would be less prone to artifacts from the flattening prior to planar biaxial tests.

The significant anisotropy of the right ventricular tissue is consistent with previous work (Ott et al., 2008) showing that both control and decellularized left ventricle were stiffer in the circumferential than longitudinal direction in equibiaxial tests and with previous studies of right ventricular properties (e.g. Ghaemi et al., 2009). Ott et al. (2008) performed biaxial tests on samples cut from cadaveric vs. decellularized left ventricle. Decellularized samples had significantly larger tangent moduli than their intact cadaveric counterparts. When adjusted for thickness, the significant difference in tangent moduli vanished, similar to our observations. Ott did not attempt to assess differences in anisotropy or heterogeneity. Figure 11 of Ghaemi et al. (2009) appears to have a ratio of about 10:1 in stress between the two directions at 20% equibiaxial strain of bovine right ventricular wall. The Ghaemi study used hooks rather than clamps, but a 10:1 stress ratio would correspond to a very large value of r in our analysis, roughly 0.8 (the exact value would depend on the results of non-equibiaxial tests). Our calculated value of $\langle r \rangle = 0.52$ for the cadaveric right ventricle samples is much lower. This difference is most likely due to our use of full-thickness samples in comparison with the use of samples extracted from the mid-one-third section of the heart by Ghaemi.

Although the decellularized tissue model is a simpler than the intact tissue, there remain questions to be considered. Variation in fiber orientation through the thickness of the myocardium (along with any contribution from the epicardium and endocardium) is particularly important. The fiber angle changes continuously transmurally through the myocardium, with the average through-thickness fiber orientation of both ventricles in the circumferential direction. In addition, both the endocardium and the epicardium exhibit higher stiffness in the circumferential direction (Kang et al., 1996; Humphrey et al., 1990). Due to the whole-organ perfusion-decellularization technique used we could not excise tissue from the midwall, as is standard for biaxial testing of ventricular tissue, for the decellularized sample group. Therefore, we tested full thickness samples from both groups, and our results must be considered as mean through-thickness descriptions. In our planar analysis, we assumed that the displacement was uniform through the tissue thickness, a reasonable but not necessarily correct assumption; further work is underway to track motion through the thickness as well as on the epicardial surface. Again, the properties calculated in this study must be seen as a transmural average of the properties of the decellularized tissue since there is no way to assess contribution from different layers.

To summarize, the current work has demonstrated that, in the right ventricle, decellularized tissue can provide a useful model of the native tissue extracellular matrix. Decellularization causes an increase in the metric describing stiffness, but when adjusted for the thickness decrease this effect is greatly reduced. There was no significant change in anisotropy or heterogeneity. A natural next step would be to apply the methods to the left ventricle (which is similar, (Humphrey, 2002; Costa et al., 2001)), where scarring and remodeling are of great interest. The GAIM technique is able to assess property variation within a tissue analog (Raghupathy et al., 2011) and, with the improved kinematic framework developed herein, it can be applied to more complex problems of ventricular tissue mechanical characterization, especially in small-animal models, for which it may be difficult if not impossible to isolate a homogeneous sample of sufficient size for biaxial testing.

Conflict of interest statement

DAT holds a financial interest in Miromatrix, Inc. and is entitled to sales royalty through the University of Minnesota for products related to the research described in this paper. This relationship has been reviewed and managed by the University in accordance with its conflict of interest policies.

Acknowledgments

This work was supported in part by the National Institutes of Health (R21-EB-009788), the Medtronic Foundation, the National Heart Lung and Blood Institute's Progenitor Cell Biology Consortium (#1U01HL100407-1), and the American Heart Association's Jon Hold DeHaan Cardiac Myogenesis Research Center (#AHA09070499N). The technical assistance of Erich Boldt in preparing and testing samples is gratefully acknowledged. We also thank the Minnesota Supercomputing Institute for the computing resources.

References

Chen, J., Song, S.K., Liu, W., McLean, M., Allen, J.S., Tan, J., Wickline, S.A., Yu, X., 2003. Remodeling of cardiac fiber structure after infarction in rats quantified with diffusion tensor MRI. American Journal of Physiology Heart and Circulatory Physiology 285 (3), H946–H954.

Costa, K.D., Holmes, J.W., McCulloch, A.D., 2001. Modelling cardiac mechanical properties in three dimensions. Philosophical Transactions: Mathematical, Physical and Engineering Sciences, 359(1783, The Integrated Heart: Modelling Cardiac Structure and Function), 1233–1250.

Cowin, S.C., Mehrabadi, M.M., 1995. Anisotropic symmetries of linear elasticity. Applied Mechanics Reviews 48 (5) 247-285.

Cox, M.A., Kortsmit, J., Driessen, N., Bouten, C.V., Baaijens, F.P., 2010. Tissue-engineered heart valves develop native-like collagen fiber architecture. Tissue Engineering. Part A 16 (5), 1527–1537.

Emery, J.L., Omens, J.H., McCulloch, A.D., 1997. Biaxial mechanics of the passively overstretched left ventricle. The American Journal of Physiology 272 (5 Pt 2), H2299–H2305.

Fomovsky, G.M., Holmes, J.W., 2010. Evolution of scar structure, mechanics, and ventricular function after myocardial infarction in the rat. American Journal of Physiology-Heart and Circulatory Physiology 298 (1), H221–H228.

Fomovsky, G.M., Thomopoulos, S., Holmes, J.W., 2010. Contribution of extracellular matrix to the mechanical properties of the heart. Journal of Molecular and Cellular Cardiology 48 (3), 490–496.

Ghaemi, H., Behdinan, K., Spence, A.D., 2009. In vitro technique in estimation of passive mechanical properties of bovine heart part I. Experimental techniques and data. Medical Engineering & Physics 31 (1), 76–82.

Humphrey, J.D., 2002. Passive Myocardium. In: Humphrey, J.D. (Ed.), Cardiovascular Solid Mechanics; Cells, Tissues, and Organs. Springer, New York, pp. 668–685.

Humphrey, J.D., Strumpf, R.K., Yin, F.C., 1990. Biaxial mechanical behavior of excised ventricular epicardium. The American Journal of Physiology 259 (1 Pt 2), H101–H108.

Kang, T., Humphrey, J.D., Yin, F.C., 1996. Comparison of biaxial mechanical properties of excised endocardium and epicardium. The American Journal of Physiology 270 (6 Pt 2), H2169–H2176.

Ott, H.C., Matthiesen, T.S., Goh, S.K., Black, L.D., Kren, S.M., Netoff, T.I., Taylor, D.A., 2008. Perfusion-decellularized matrix: using nature's platform to engineer a bioartificial heart. Nature Medicine 14 (2), 213–221.

Raghupathy, R., Barocas, V.H., 2009. A closed-form structural model of planar fibrous tissue mechanics. Journal of Biomechanics 42 (10), 1424–1428.

Raghupathy, R., Barocas, V.H., 2010. Generalized anisotropic inverse mechanics for soft tissues. Journal of Biomechanical Engineering 132 (8), 081006.

Raghupathy, R., Witzenburg, C., Lake, S.P., Sander, E.A., & Barocas, V.H., 2011. Identification of regional mechanical anisotropy in soft tissue analogs. Journal of Biomechanical Engineering 133 (9), 091011.

Sacks, M.S., Chuong, C.J., 1993. Biaxial mechanical properties of passive right ventricular free wall myocardium. Journal of Biomechanical Engineering 115 (2), 202–205.

Thomson, W., 1856. Elements of a mathematical theory of elasticity. Philosophical Transactions of the Royal Society of London 146, 481–498.

Wainwright, J.M., Czajka, C.A., Patel, U.B., Freytes, D.O., Tobita, K., Gilbert, T.W., Badylak, S.F., 2010. Preparation of cardiac extracellular matrix from an intact porcine heart. Tissue Engineering.Part C, Methods 16 (3), 525–532.

Wang, B., Borazjani, A., Tahai, M., Curry, A.L., Simionescu, D.T., Guan, J., To, F., Elder, S.H., Liao, J., 2010. Fabrication of cardiac patch with decellularized porcine myocardial scaffold and bone marrow mononuclear cells. Journal of Biomedical Materials Research. Part A 94 (4), 1100–1110.

Weymann, A., Loganathan, S., Takahashi, H., Schies, C., Claus, B., Hirschberg, K., Soos, P., Korkmaz, S., Schmack, B., Szabo, G., 2011. Development and evaluation of a perfusion decellularization porcine heart model—generation of 3-dimensional myocardial neoscaffolds. Circulation Journal: Official Journal of the Japanese Circulation Society 75 (4), 852–860.